biomass

MDPI

Article

Evaluation of Heavy Metal Adsorption Efficiency of Biochars Derived from Agricultural Waste

Velyana Georgieva [1], Lenia Gonsalvesh [1,2,*], Sonia Mileva [1], Mariyana Hamanova [3] and Hyusein Yemendzhiev [4]

[1] Department of Chemistry, Burgas State University "Prof. Dr. Asen Zlatarov", 1 Y. Yakimov Blvd, 8010 Burgas, Bulgaria; velyana_topalska@btu.bg (V.G.); sonyamileva1708@abv.bg (S.M.)
[2] Central Scientific Research Laboratory, Burgas State University "Prof. Dr. Asen Zlatarov", 1 Y. Yakimov Blvd, 8010 Burgas, Bulgaria
[3] Cleantech Bulgaria Foundation, 11 Lukashov Str., Floor 6, 3000 Vratsa, Bulgaria; mariyana@cleantech.bg
[4] Department of Chemical Technologies, Burgas State University "Prof. Dr. Asen Zlatarov", 1 Y. Yakimov Blvd, 8010 Burgas, Bulgaria; hyemendzhiev@btu.bg
* Correspondence: lenia_gonsalvesh@abv.bg or lenia_gonsalvesh@uniburgas.bg

Abstract: This study investigates the potential of biochars derived from agricultural waste biomass for the removal of heavy metal ions from aqueous solutions. Biochars were produced via slow pyrolysis at 793 K using almond shells (AS), walnut shells (WS), pistachio shells (PS), and rice husks (RH) as feedstocks. The physicochemical properties and adsorption performance of the resulting materials were evaluated with respect to Cd(II), Mn(II), Co(II), Ni(II), Zn(II), total Iron (Fe_{tot}), total Arsenic (As_{tot}), and total Chromium (Cr_{tot}) in model solutions. Surface morphology, porosity, and surface chemistry of the biochars were characterized by scanning electron microscopy (SEM), nitrogen adsorption at 77 K (for specific surface area and pore structure), Fourier-transform infrared spectroscopy (FTIR), and determination of the point of zero charge (pH_{pzc}). Based on their textural properties, biochars derived from WS, PS, and AS were classified as predominantly microporous, while RH-derived biochar exhibited mesoporous characteristics. The highest Brunauer–Emmett–Teller (S_{BET}) surface area was recorded for PS biochar, while RH biochar showed the lowest. The pistachio shell biochar exhibited the highest specific surface area (440 m^2/g), while the rice husk biochar was predominantly mesoporous. Batch adsorption experiments were conducted at 25 °C, with an adsorbent dose of 3 g/L and a contact time of 24 h. The experiments in multicomponent systems revealed removal efficiencies exceeding 87% for all tested metals, with maximum values reaching 99.9% for Cd(II) and 97.5% for Fe_{tot}. The study highlights strong correlations between physicochemical properties and sorption performance, demonstrating the suitability of these biochars as low-cost sorbents for complex water treatment applications.

Keywords: biochars; adsorption; heavy metals removal

check for updates

Academic Editor: Kaveh Khalilpour

Received: 6 April 2025
Revised: 23 May 2025
Accepted: 27 May 2025
Published: 3 June 2025

Citation: Georgieva, V.; Gonsalvesh, L.; Mileva, S.; Hamanova, M.; Yemendzhiev, H. Evaluation of Heavy Metal Adsorption Efficiency of Biochars Derived from Agricultural Waste. *Biomass* **2025**, *5*, 33. https://doi.org/10.3390/biomass5020033

Copyright: © 2025 by the authors. Licensee MDPI, Basel, Switzerland. This article is an open access article distributed under the terms and conditions of the Creative Commons Attribution (CC BY) license (https://creativecommons.org/licenses/by/4.0/).

1. Introduction

Heavy metal pollution is a major global environmental concern due to the non-biodegradable nature of these elements, their persistence in soils and natural waters for decades, and the challenges and costs associated with their removal from contaminated environments. Based on their toxicological effects on human health, heavy metals are commonly categorized into three groups [1]: highly toxic metals such as cadmium, arsenic, mercury, lead, and chromium [2]; metals with harmful but less severe effects including cobalt, nickel, molybdenum, copper, and zinc; and elements with relatively low toxicity

such as barium, vanadium, manganese, aluminum, and strontium. While elements such as iron, manganese, and zinc are essential for metabolic functions, their accumulation at elevated levels can disrupt biological systems and pose serious health risks, including organ dysfunction and oxidative stress.

Several of these elements—including cobalt (Co), copper (Cu), chromium (Cr), iron (Fe), magnesium (Mg), manganese (Mn), molybdenum (Mo), nickel (Ni), and zinc (Zn)—are essential trace elements required for the proper functioning of living organisms [2]. However, more than 90% of their environmental presence is attributed to anthropogenic sources and industrial development [3]. These metals can enter the human body via ingestion, inhalation, or dermal contact, potentially leading to serious health issues.

For instance, elevated cadmium exposure can cause skeletal deformities, cognitive impairment in children, severe back pain, and the onset of "itai-itai" disease [4,5]. Arsenic has been linked to cardiovascular and peripheral vascular diseases, developmental abnormalities, neurological and neurobehavioral disorders, diabetes, hearing loss, hematological conditions (e.g., anemia, leukopenia, eosinophilia), and various forms of cancer [2]. Manganese toxicity can lead to symptoms resembling Parkinson's disease, "manganese rickets," and respiratory illnesses such as pulmonary embolism, pneumonia, and bronchitis [6]. Nickel exposure is associated with joint degeneration, spinal cord paralysis, pulmonary fibrosis, and cardiovascular and renal dysfunctions [7,8]. Among the most serious consequences of heavy metal accumulation in the human body is their carcinogenic potential, which may trigger malignant tumor formation in various organs [2,4,6–8].

Numerous regulatory frameworks governing air, water, and soil quality have been developed to limit environmental contamination and its harmful effects on ecosystems. The concentration limits for the investigated elements are not uniform and depend on their toxicological profiles and regulatory context. The reference concentration limits for selected metal ions investigated in this study correspond to the parametric values established in the European Union Drinking Water Directive (Directive (EU) 2020/2184). For cadmium (Cd), chromium (Cr), and nickel (Ni), the directive sets binding maximum allowable concentrations of 5 μg/L, 50 μg/L, and 20 μg/L, respectively, due to their toxicological relevance. In contrast, iron (Fe) is listed as an indicator parameter, with a reference value of 200 μg/L, reflecting its impact on the organoleptic properties of drinking water rather than direct health effects. These regulatory thresholds provide a scientifically grounded framework for assessing the environmental and public health significance of the experimental results. For other metals included in this study, such as manganese (Mn), zinc (Zn), cobalt (Co), and arsenic (As), the European Union Drinking Water Directive (2020/2184) does not specify binding parametric values. In such cases, internationally recognized guidelines, particularly those issued by the World Health Organization, are often used as reference. For example, the WHO 2017 recommends a provisional guideline value of 10 μg/L for arsenic in drinking water, due to its well-documented toxicity and carcinogenic potential.

Conventional treatment methods—such as chemical precipitation, ion exchange, membrane separation, flotation, and electrocoagulation—have been extensively applied for heavy metal removal from wastewater [9]. However, these methods often suffer from limitations such as long treatment times, incomplete contaminant removal, high costs for equipment and reagents, and the generation of toxic sludge that requires further treatment [10]. In recent years, adsorption has gained attention as an effective and promising alternative for the removal of heavy metal ions from aqueous media. The main constraint to large-scale implementation lies in the high commercial cost of available adsorbents and the challenge of their regeneration for repeated use.

Another pressing environmental issue is the generation and accumulation of vast quantities of waste, which calls for the urgent development of sustainable strategies for waste management. One of the sectors known for substantial waste production is agriculture. Agricultural waste is typically burned, landfilled, or incorporated into soil to improve its structure; however, these practices are often inefficient and, in some cases, restricted by environmental regulations. Due to their high carbon content, biomass wastes are increasingly being converted through pyrolysis—a thermochemical process carried out in an oxygen-deficient atmosphere. Pyrolysis yields high-energy gases (both condensable and non-condensable) suitable for fuel or chemical feedstocks, and a solid fraction (char) that can be used as a soil amendment, adsorbent, catalyst, or further upgraded to activated carbon (AC) through physical or chemical activation [11,12].

Thanks to their wide availability and low economic value, biomass wastes are regarded as sustainable, eco-friendly, and cost-effective feedstocks for the production of valuable pyrolyzed materials.

Low-cost adsorbents derived from agro-biological wastes—such as kola nut shells, sugarcane bagasse, potato peels, rice husk ash, lentil shells, sargassum spp., hazelnut shells, coconut, almond, walnut, and peanut shells—have been successfully used to purify aqueous solutions contaminated with a variety of pollutants [10,13–15]. Some of these materials have even been evaluated for the simultaneous removal of multiple heavy metal ions. The properties and efficiency of these bio-based adsorbents vary depending on factors such as geographic origin, plant species, and processing conditions, all of which influence their morphology, porosity, and chemical composition.

The aim of this study is to produce and characterize biochars derived from selected agricultural waste materials—namely almond shells (AS), walnut shells (WS), pistachio shells (PS), and rice husks (RH)—and to systematically evaluate their performance in the adsorption of multiple heavy metal ions from complex aqueous solutions. By employing a comparative approach, the study seeks to elucidate the relationship between the physicochemical properties of the biochars—including surface morphology, pore structure, surface chemistry, and surface charge—and their adsorption efficiency and selectivity toward Cd(II), Mn(II), Co(II), Ni(II), Zn(II), total iron (Fe_{tot}), total arsenic (As_{tot}), and total chromium (Cr_{tot}). The biochars were produced via slow pyrolysis and characterized using scanning electron microscopy, nitrogen adsorption measurements, FTIR spectroscopy, and determination of the point of zero charge. Batch adsorption experiments were conducted in multicomponent aqueous systems under environmentally relevant conditions and optimized pH values, allowing for a realistic assessment of sorbent performance. The scientific contribution of this work is rooted in its direct comparison of four biomass-derived sorbents, tested under identical conditions for the simultaneous removal of both cationic and anionic species—a relatively rare approach in the current literature. Unlike studies focusing on single-metal systems, this research addresses the complexity of real wastewater and provides new insights into the interdependence between material characteristics and adsorption behavior. The results establish clear correlations between porosity, surface functionality, and electrostatic properties, and the removal efficiency for individual ions, offering a solid foundation for the design of optimized, low-cost sorbents for sustainable water treatment applications.

2. Materials and Methods

2.1. Adsorbents

The agro-biological wastes used in this study included almond shells (AS), pistachio shells (PS), walnut shells (WS), and rice husks (RH). Most of the samples were collected from agricultural plantations located in the Thracian Plain, Bulgaria. Prior to pyrolysis,

the raw materials were washed with distilled water, air-dried at room temperature for 24 h, ground using a high-speed ball mill, and sieved to obtain particles smaller than 2 mm. The pyrolysis was carried out in an electric muffle furnace (model LM 312.11, MLM Elektro, Bad Frankenhausen, Germany) under a nitrogen atmosphere. Nitrogen gas (purity: 99.9 vol.%) was continuously supplied at a constant flow rate to ensure an inert environment. The temperature program involved a heating rate of 15 K/min up to 793 K, followed by an isothermal period of 1 h at the final temperature. The resulting biochars were sieved, and the particle size fraction between 63 and 250 μm was selected for subsequent adsorption experiments.

In order to investigate the surface morphology of biochars, scanning electron microscopy was applied using a high vacuum SEMoscope IEM11 (Inovenso, Istanbul, Turkey).

The porous structure characterization was carried out by measuring nitrogen adsorption isotherms at 77 K on an automatic apparatus Surfer (Thermo Fisher Scientific, Waltham, MA, USA. The specific surface area of biochars was determined by using N_2 adsorption data in the range of relative pressures 0.05–0.28 (for isotherms of type IV) or in a range of relative pressures determined by the criteria of Rouquerol (for isotherms of type I) and the linear form of BET equation [16,17]. The total pore volume, known as volume of Gurvich, $V_{0.95}$, was determined based on the volume of adsorbate, recorded on the desorption branch of the adsorption isotherm at a relative pressure $P_i/P_o = 0.95$. The micropore volume (V_{micro}) was calculated by using the Dubinin-Radushkevich equation up to $P_i/P_o \leq 0.16$ [18], while mesopore volume (V_{meso}) was calculated as the difference between $V_{0.95}$ and V_{micro}. The mean (r_p) and maximal (r_{max}) pore radii were computed by different calculation procedures, i.e., Horvart–Kawazoe (HK, for microporous) and Barrett–Joyner–Halenda (BJH, for mesoporous) [18].

FTIR spectroscopy in the range 4000–400 cm^{-1} was applied using a Nicolet iS 50 spectrophotometer (Thermo Fisher Scientific, Waltham, MA, USA) to obtain information about surface functional groups of the samples under consideration.

2.2. Adsorbates

All chemicals used were of analytical grade (≥99% purity) and sourced from certified suppliers. Single-element standard solutions containing Cd(II), Mn(II), Co(II), Ni(II), Zn(II), Fe(III), As(V), and Cr(VI) in concentration of 1000 mg/L, were prepared by dissolving a certain amount of the corresponding salts (chlorides or nitrates) in ultrapure water. The multicomponent aqueous solutions prepared for the adsorption study were with a dominant concentration of Cd(II) and Fe(III) ions, i.e., 5 and 7 mg/L, respectively, and with a lower concentration of Cr(VI), Mn(II), Co(II), Ni(II), Zn(II), As(V), i.e., 50, 100, 5, 50, 500, 10 μg/L, respectively. The content of the heavy metal ions in the solutions before and after adsorption was analyzed using a mass spectrometer, ICP MS model ICAP Q (Thermo Fisher Scientific, Waltham, MA, USA), according to BDS EN ISO 17294-2: 2016 [19].

2.3. Adsorption Study

The values of pH_{pzc} of the adsorbents were determined by mixing 250 mg biochar with 10 mL freshly boiled and cooled ultrapure water as described in [20]. The mixture was stirred by a magnetic stirrer for 48 h at room temperature. The pH values of the solutions measured by pH-meter model Inolab pH 7110 (WTW, Weilheim, Germany) after 48 h were considered as the pH_{pzc} values of the biochars.

The adsorption experiments were carried out at various pH (2.5–8.5), aforementioned concentrations of considered heavy metals in the multicomponent solution, temperature of 25 °C, adsorbent dose of 3 g/L, and the contact time of 24 h (the established equilibrium state). The selected pH range (2.5–8.5) was chosen based on published solubility data to

avoid hydrolysis and precipitation of metal hydroxides. The various pH values of the solutions were adjusted by adding either 0.1 M HCl or 0.1 M NaOH to the initial solutions. The adsorption was performed in an iodine flask of 200 cm^3, containing 100 cm^3 of the solution under examination and the required amount of adsorbent, placed into a water bath, (Memmert WB22 Schwabach, Germany), and equipped with a shaking system (Memmert WB22 (Schwabach, Germany). The temperature was maintained with an accuracy of ±0.5 °C. To prevent precipitation, all adsorption experiments were conducted at pH values below 9, where metal ion speciation remained predominantly soluble and stable in aqueous media.

The removal of heavy metal ions by the adsorbents, expressed in %, and the amount of ions adsorbed per unit weight of adsorbents at the equilibrium state (adsorption capacity), in mg/g, were calculated using the following equations:

$$\% \text{ removal of ions} = \frac{C_0 - C_e}{C_0} \times 100 \quad (1)$$

$$Q_e = \frac{C_0 - C_e}{m} V \quad (2)$$

where C_0 (mg/L) is the initial concentration of the metal ion in solution, C_e (mg/L) is the equilibrium concentration after adsorption, V (L) is the volume of the solution, and m (g) is the mass of the adsorbent used. The removal efficiency (%) was calculated by Formula (1), and the adsorption capacity at equilibrium, Q_e (mg/g), was calculated by Formula (2).

Each adsorption experiment was conducted in two independent replicates to ensure reproducibility. The obtained results were highly consistent across repetitions, and the mean values are presented herein.

3. Results

3.1. Adsorbents Characterization

The surface morphology of biochars from RH, WS, AS, and PS is represented in SEM images (Figure 1). Almond shell biochar (Figure 1A) possesses a three-dimensionally ordered porous structure with macropores of about 24 μm, acting as transport arteries to micro- and mesopores [21]. A similar macroporous structure is observed for PS biochar (Figure 1C), but with macropore sizes up to 20 μm. Walnut biochar (Figure 1B) shows an irregular and inhomogeneous surface with poor macropore distribution. The morphology of rice husk biochar (Figure 1D) reflects the skeletal structure of the precursor [22,23].

Nitrogen adsorption isotherms at 77 K (Figure 2) show that AS, WS, and PS biochars exhibit a steep rise at low relative pressures, a sharp knee around $P_i/P_o \approx 0.01$, and nearly horizontal behavior at medium to high relative pressures, indicating predominantly microporous structures. RH-BC (Figure 2D), in contrast, shows a type IV isotherm and H-3 hysteresis loop (according to IUPAC classification), indicating a mesoporous and biporous structure. Such hysteresis is typical of toroidal pores, bottle-shaped pores with narrow necks, or wedge-shaped pores [22,23].

Textural characteristics calculated via various methods are presented in Table 1. PS-BC shows the highest surface area (440 m^2/g), while RH-BC has the lowest (S_{BET} = 149 m^2/g). More than 77% of the pore volume in AS, WS, and PS biochars is attributed to micropores, whereas RH-BC is predominantly mesoporous (V_{mezo} = 77%).

The surface chemistry of the biochars was studied via FTIR (Figure 3). Raw and pyrolyzed samples exhibit absorption bands in the 3420–3450 cm^{-1} region, attributed to O–H stretching in alcoholic, phenolic, and carboxyl groups [24]. Peaks near 2925 and 2860 cm^{-1} correspond to symmetric and asymmetric C–H stretching [13]. The 1740–1700 cm^{-1} bands relate to non-ionic carboxyl groups (-COOH, -$COOCH_3$), indicating carboxylic acids or

esters [25]. Aromatic skeletal vibrations and C=C stretching appear between 1620 and 1422 cm^{-1}, and C–O vibrations are found between 1320 and 1210 cm^{-1} [26].

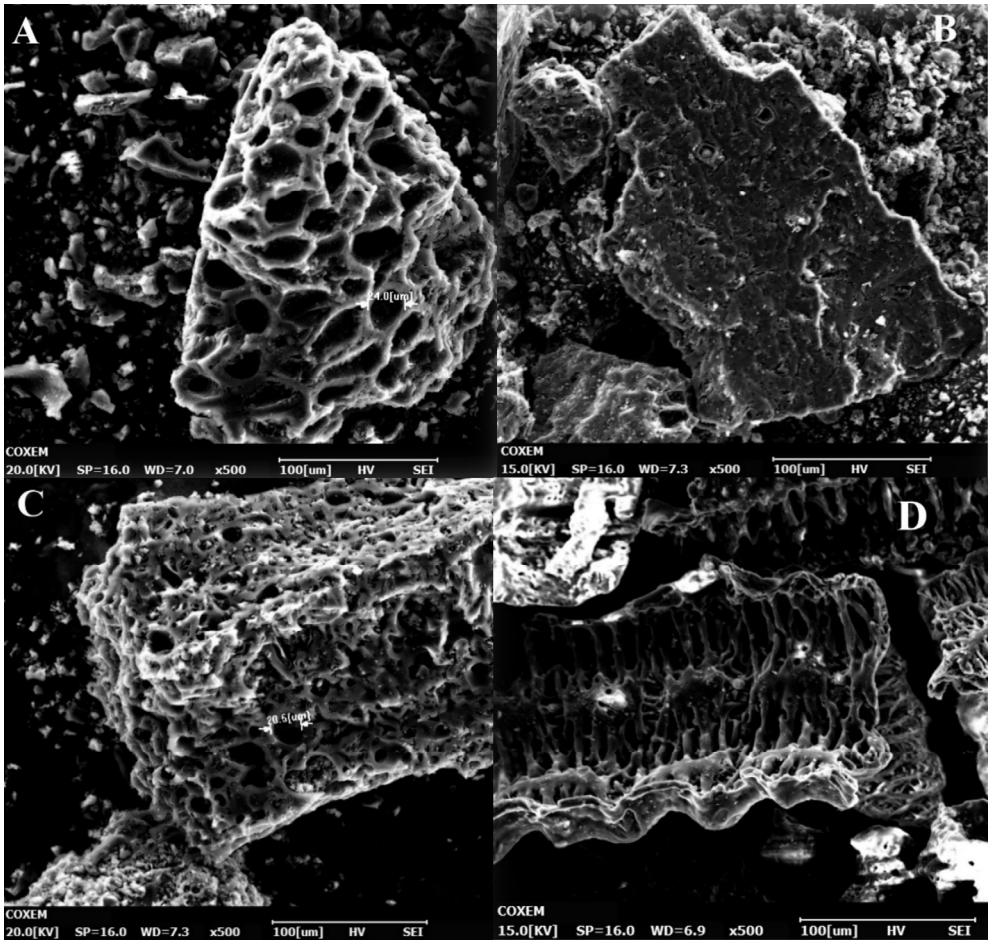


Figure 1. SEM images of biochars from (**A**)—almond shells, (**B**)—walnut shells, (**C**)—pistachio shells, and (**D**)—rice husks.

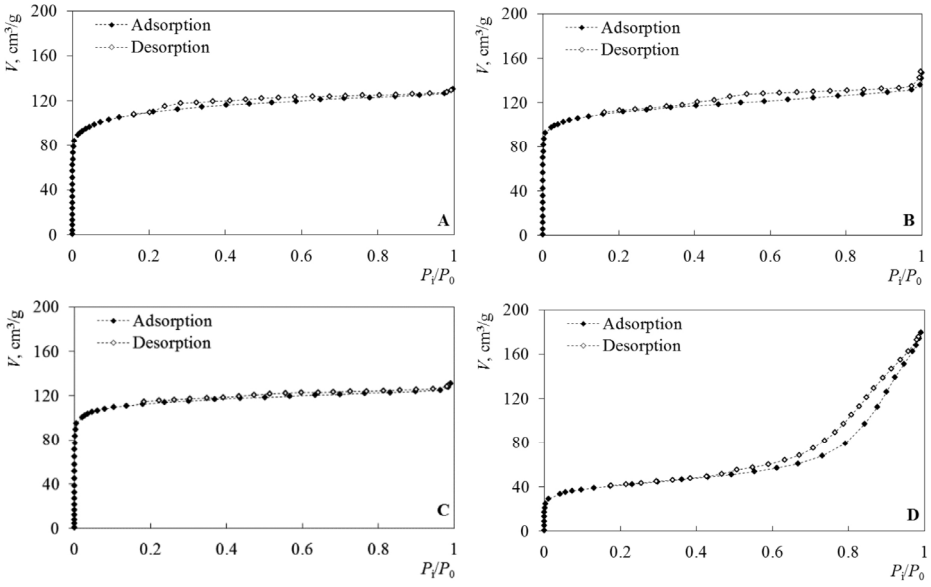


Figure 2. Adsorption-desorption isotherms of biochars from (**A**)—almond shells, (**B**)—walnut shells, (**C**)—pistachio shells, and (**D**)—rice husks.

Table 1. Textural characteristics of biochars from almond shells (AS-BC), walnut shells (WS-BC), pistachio shells (PS-BC), and rice husks (RH-BC).

Calculation Procedure	Parameters	Biochars			
		AS-BC	**WS-BC**	**PS-BC**	**RH-BC**
BET	$V_{0.95}$, cm^3/g	0.1948	0.1605	0.1932	0.2365
	C	4828	629	2509	486
	S_{BET}, m^2/g	404	332	440	149
	R	0.9997	0.9998	0.9999	0.9999
HK or BJH	r_p, nm	0.29	1.90	0.29	5.40
	r_{max}, nm	0.29	1.30	0.30	4.10
DR	V_{micro}, cm^3/g	0.1619	0.1243	0.1672	0.0544
	V_{mezo}, cm^3/g	0.0329	0.0362	0.0258	0.1821
	V_{micro}, %	83.0	77.4	86.5	23.0
	V_{mezo}, %	17.0	22.6	13.5	77.0

BET—Brunauer–Emmett–Taylor, HK—Horvart–Kawazoe (for microporous), BJH—Barrett–Joyner–Halenda (for mesoporous), DR—Dubinin–Radushkevich.

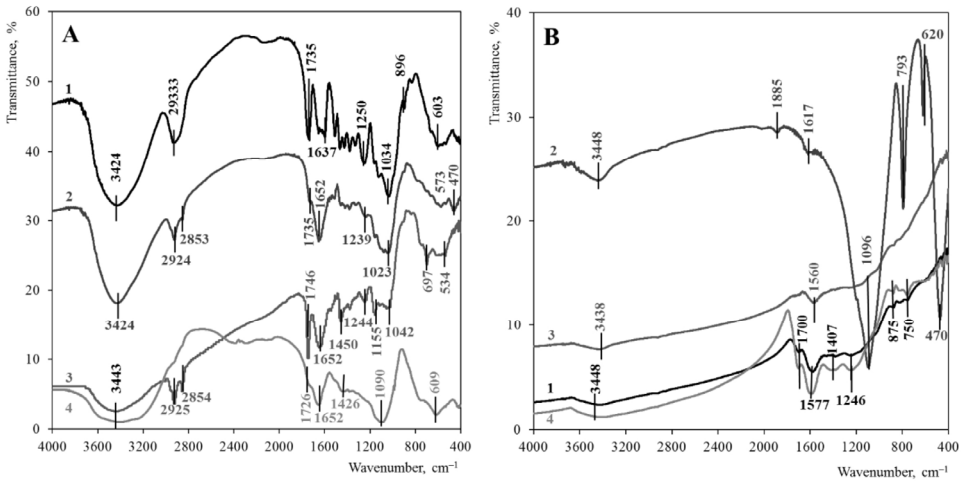


Figure 3. FTIR spectra of raw (**A**) and pyrolyzed (**B**) agrobiological wastes: 1—almond shells, 2—rice husks, 3—pistachio shells, and 4—walnut shells.

Post-pyrolysis spectra (Figure 3B) show reduced or vanished C–H bands (2920–2860 cm^{-1}) and generally decreased intensity in other regions, consistent with thermal degradation of cellulose, hemicellulose, and lignin [24]. RH-BC shows strong Si–O bands at 1096, 793, and 470 cm^{-1}, corresponding to Si–O and O–Si–O vibrations [27].

3.2. pH_{pzc} and Surface Charge

The pH_{pzc} values of biochars (Table 2) indicate that in the studied pH range (2.5–8.5), most surfaces remain positively charged. WS-BC becomes negatively charged above pH 6.0, and AS-BC above pH 8.0.

Table 2. The values of pH_{pzc} of the studied adsorbents.

Adsorbents	pH_{pzc}
RH-BC	9.630
PC-BC	8.710
AS-BC	8.083
WS-BC	6.036

3.3. Adsorption Efficiency and Capacity

The effect of pH on metal adsorption was evaluated in the range 2.5–8.5 (to avoid metal precipitation above pH 9). Adsorption trends for AS-BC are shown in Figure 4. At pH 2.5, Mn and Cd adsorption is suppressed, while Cr, As, and Zn are efficiently removed (>80%). As pH increases, the removal of Fe, Mn(II), Co(II), Ni(II), and Cd(II) improves.

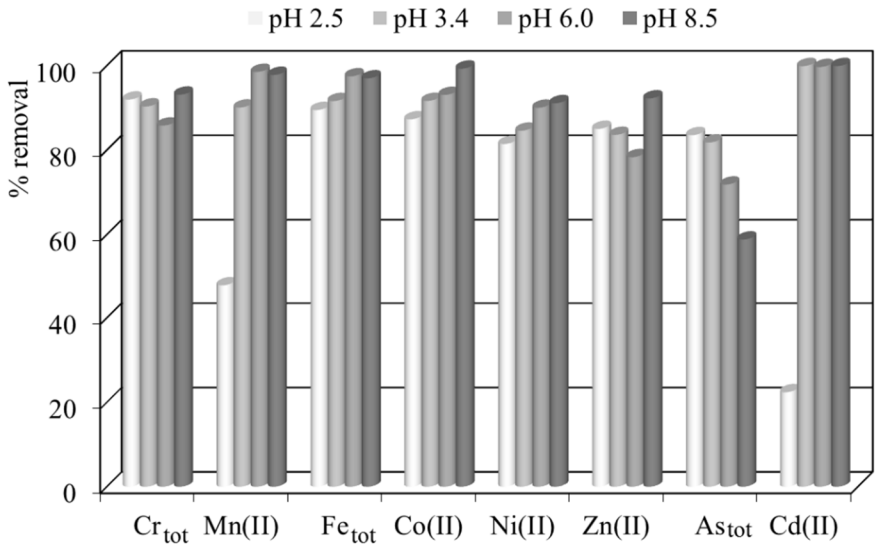


Figure 4. The effect of pH on the adsorption of heavy metal ions onto almond shells biochar at 25 °C, 3 g/L adsorbent dose, and 24 h contact time in model solutions.

Zn(II) speciation [28] indicates that Zn^{2+} dominates up to pH 7, while precipitation begins at pH 8.5. At pH 6.5, Cr(VI) species become prevalent [29], supporting strong electrostatic attraction between CrO_4^{2-} and the positively charged adsorbent. For AS-BC, pH 6.0 is optimal for multicomponent removal (except Zn, As, and Cr).

WS-BC (Figure 5) shows increased adsorption with rising pH, except for As. Acidic conditions favor anionic adsorption via electrostatic attraction. WS-BC performs well at pH 6.0 for all metals except As.

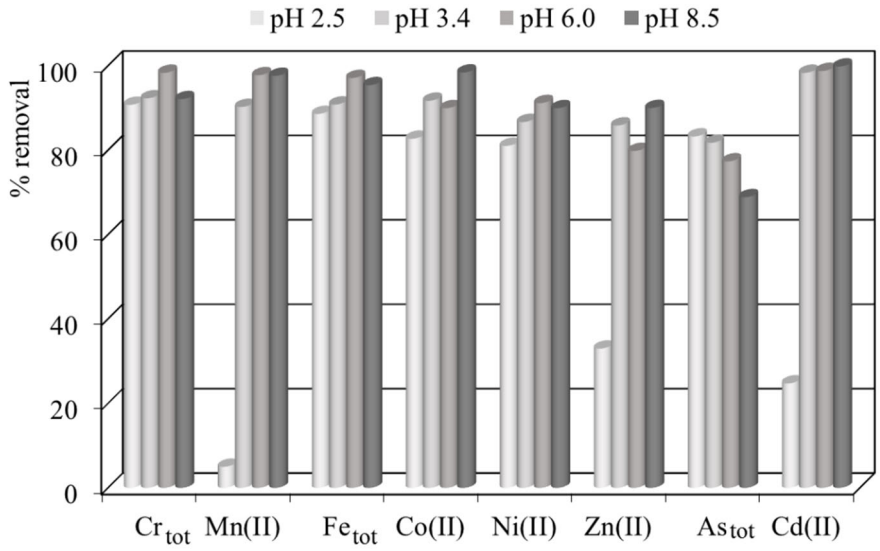


Figure 5. The pH influence on the heavy metal ions adsorption by walnut shells biochar at 25 °C, 3 g/L adsorbent dose, and 24 h contact time in model solutions.

PS-BC (Figure 6) shows reduced As and Co adsorption with rising pH. Zn(II) removal drops at pH 8.5 due to PS-BC's surface charge and $Zn(OH)^+$ formation. Optimal metal removal occurs at pH 6.0, excluding As.

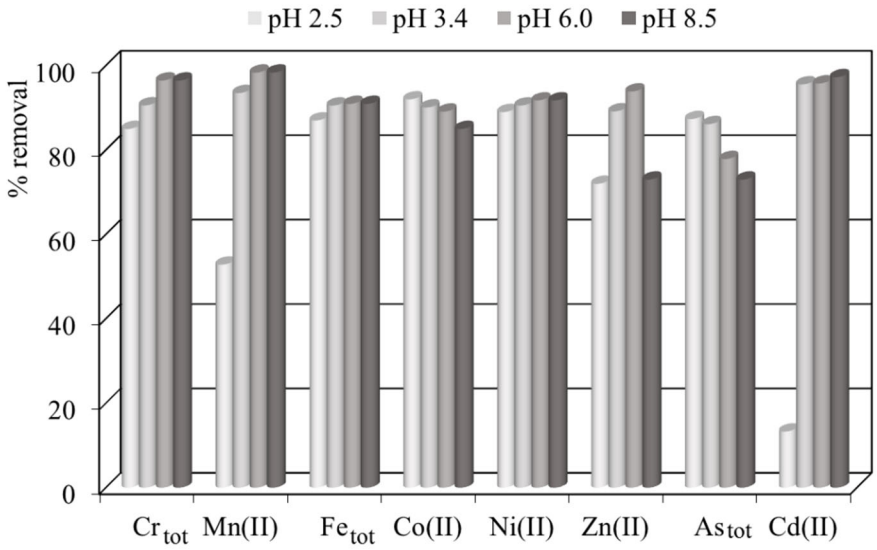


Figure 6. The effect of pH on the heavy metal ions adsorption onto biochar from pistachio shells at 25 °C, 3 g/L adsorbent dose, and 24 h contact time in model solutions.

RH-BC (Figure 7) shows reduced Mn and Cd adsorption in acidic media, with increased removal of most metals as pH rises. As and Cr show exceptions. Optimal RH-BC performance is seen at pH 6.0.

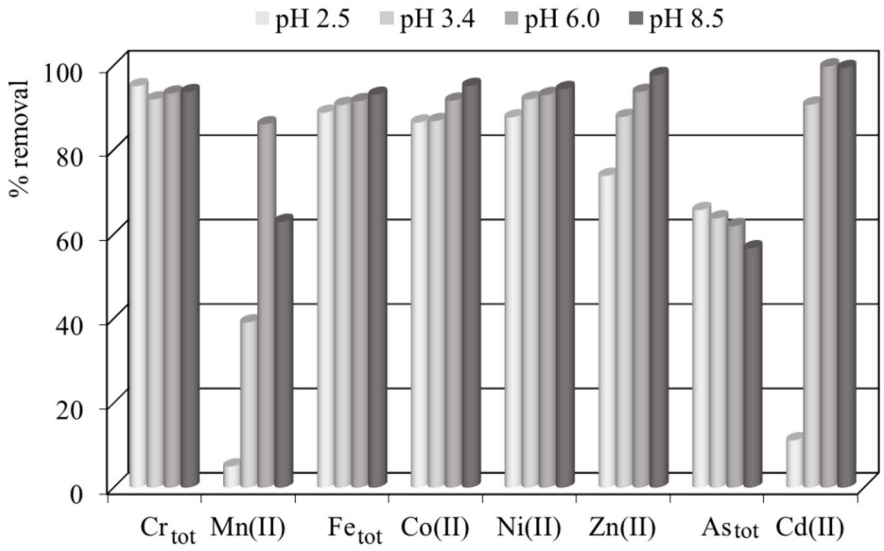


Figure 7. The effect of pH on the heavy metal ions adsorption onto biochar from rice husks at 25 °C, 3 g/L adsorbent dose, and 24 h contact time in model solutions.

Adsorption efficiency comparisons reveal peak removals for the following: As at pH 2.5 (87.35%, PS-BC); Cd at pH 3.4 (99.90%, AS-BC); Cr at pH 6 (98.35%, WS-BC); Mn at pH 6 (98.52%, AS-BC); Fe at pH 6 (97.47%, AS-BC); Co at pH 8.5 (99.29%, AS-BC); Ni at pH 8.5 (94.41%, RH-BC); Zn at pH 8.5 (97.73%, RH-BC). Clearly, the overall removal efficiencies range from 87.4% to 99.9%, depending on adsorbent and pH. Literature comparisons show lower performance in other studies (e.g., Niazi et al. [30]; Lima et al. [31]).

Adsorption capacity trends reveal the highest Q_e values for Fe_{tot}, followed by Cd(II). Among the adsorbents, WS-BC, AS-BC, and RH-BC exhibit comparable Fe_{tot} adsorption capacities, which increase slightly with pH: Q_e = 2.17 ± 0.01 mg/g at pH 2.0; Q_e = 2.18 ± 0.02 mg/g at pH 3.4; Q_e = 2.29 ± 0.07 mg/g at pH 6.0; and Q_e = 2.39 ± 0.04 mg/g at pH 8.5. PS-BC shows similar Fe_{tot} adsorption below pH 6.0 but a drop at pH 8.5. For Cd(II), all adsorbents perform well between pH 3.4 and 8.5 ($Q_e \approx 1.75 \pm 0.05$ mg/g). Maximum capacities and optimal pH values are in Table 3.

Table 3. Maximum adsorption capacities of target metals.

Ions	Adsorbent	Q_e, mg/g	pH Medium
Cr_{tot}	RH-BC	0.018	2.5
Mn(II)	WS-BC	0.053	8.5
Fe_{tot}	WS-BC	2.419	8.5
Co(II)	WS-BC	0.002	8.5
Ni(II)	RH-BC	0.021	3.4
Zn(II)	RH-BC	0.164	3.4
Astot	PS-BC	0.003	2.5
Cd(II)	WS-BC	1.820	3.4

Note: The adsorption capacities (Q_e, mg/g) represent experimentally determined equilibrium values obtained under optimized pH conditions for each ion. These values are not derived from isotherm model fitting. Due to differences in initial concentrations and ion-specific solution behavior, these values should not be used for direct comparison across metals. Meaningful comparisons are limited to evaluating the performance of different sorbents for a given metal.

4. Discussion

The surface characteristics and pore structures of the resulting biochars are closely related to the physicochemical nature of the original biomass. Almond, walnut, and pistachio shells, being dense lignocellulosic materials, exhibit varying degrees of rigidity, lignin content, and cellular compactness, which directly influence their pyrolytic behavior and the development of porous carbon frameworks. In general, a higher lignin content and greater mechanical integrity tend to promote the formation of thermally stable biochars with well-developed micro- and mesoporosity. The presence of inherent mineral elements such as calcium, potassium, and magnesium may further assist in pore generation through catalytic effects during pyrolysis. Among the studied materials, PS-derived biochar exhibited the highest specific surface area and the most pronounced microporosity. These characteristics are instrumental in enhancing the adsorption performance, particularly under competitive multicomponent conditions. The structural properties of the pistachio shell precursor, including its relatively high lignin content and mechanical integrity, likely contributed to the formation of stable and highly porous carbonaceous structures during pyrolysis. While these findings suggest that pistachio shell biomass may offer advantageous properties for producing high-performance porous biochars, further comparative studies are needed to confirm and better understand the underlying mechanisms. The microporosity observed in AS, WS, and PS biochars aligns with the steep initial rise in nitrogen isotherms. RH-BC's distinct mesoporosity and H-3 hysteresis loop reflect its silica content and unique pore geometry [22,23]. Although RH-derived biochar showed the lowest specific surface area among the tested materials, it demonstrated notable adsorption efficiency for Ni(II) and Zn(II). This behavior may be explained by its mesoporous nature and the high silica content of rice husks, which could facilitate the diffusion and retention of larger hydrated metal ions. The presence of silica may also influence surface charge distribution and ion-exchange interactions, further contributing to the adsorption process. The highly porous structure of AS and PS biochars, particularly PS-BC, likely accounts for their superior surface areas and higher adsorption efficiencies.

FTIR spectra confirm the progressive degradation of organic functional groups during pyrolysis [24], reducing the number of polar sites but increasing carbonaceous structure, beneficial for hydrophobic interactions and π–π bonding. RH-BC's unique silica peaks [27] further differentiate it chemically from the other biochars.

$pH_{pz}c$ values provide insight into the electrostatic interactions governing adsorption. Below pH_{pzc}, the adsorbent surface is protonated, favoring the adsorption of anionic species (e.g., Cr(VI), As(V)). This explains why the As removal peaks at low pH. In contrast, cationic species like Fe(III), Ni(II), and Cd(II) are better adsorbed at higher pH levels due to decreased competition with H^+ and favorable electrostatic interactions.

The pH-dependent adsorption behavior reflects the combined influence of metal ion speciation and the surface charge properties of the biochars. The optimal adsorption pH for most ions was 6.0, indicating a favorable balance between surface charge and metal speciation. At lower pH values, the biochar surfaces are protonated, favoring the adsorption of anionic species such as Cr(VI) and As(V) through electrostatic attraction. In contrast, the removal efficiency for cationic metals, including Mn(II), Co(II), and Ni(II), improves with increasing pH, due to the progressive deprotonation of surface functional groups and reduced competition from protons for binding sites. This trend is also evident in the case of Cd(II), whose adsorption at pH 3.4 aligns with its prevalent ionic form and minimal precipitation. Likewise, the adsorption of Fe(III) and Mn(II) increases with rising pH as a result of diminished proton interference. These adsorption trends are in line with the expected aqueous speciation of the studied metal ions. Under acidic to neutral pH conditions, Cr(VI) exists mainly as $HCrO_4^-$ and CrO_4^{2-}, while As(V) is present predominantly as $H_2AsO_4^-$ and $HAsO_4^{2-}$. These anionic species interact favorably with the positively charged biochar surfaces at lower pH, which explains the enhanced removal of Cr(VI) and As(V) in acidic media. In contrast, Cd(II), Mn(II), Co(II), Ni(II), and Fe(III) remain in solution as hydrated cations at lower pH, with adsorption improving at higher pH due to surface deprotonation and reduced competition from H^+ ions. However, for Fe(III) and to some extent for Mn(II), hydrolysis becomes significant above pH 6.5–7, leading to the formation of soluble complexes such as $Fe(OH)_2^+$ and $Fe(OH)_3^0$, or even precipitation of $Fe(OH)_3$(s). Similar effects may occur for other cations at elevated pH levels. To avoid the confounding influence of precipitation, the experimental pH range was limited to 2.5–8.5. Adsorption behavior above this threshold was not evaluated, as precipitation could dominate and obscure the interpretation of true adsorption mechanisms.

Comparison with literature (e.g., Niazi et al. [30]; Lima et al. [31]; others [32–34]) shows that the biochars produced here outperformed several conventional biomass-derived adsorbents, particularly under multicomponent conditions. Notably, the AS-BC biochar showed high performance across multiple ions, and WS-BC excelled at Fe_{tot} and Cd removal. Although the reported equilibrium adsorption capacities (Q_e) may seem modest, this is a direct consequence of the experimental design, which employed environmentally relevant, low initial concentrations of metal ions in multicomponent aqueous systems. As defined by the equation 2, adsorption capacity is inherently dependent on the starting concentration. Lower Q_e values under such realistic conditions are expected and reflect the practical performance of the biochars. It is important to note that Q_e values presented for different metal ions are not directly comparable to one another, as they are influenced by distinct initial concentrations, ionic properties, complexation behavior in solution, and varying degrees of sorbent surface saturation. The values are therefore interpreted in the context of intra-metal comparisons among biochars tested under identical conditions. This approach allows for a valid assessment of sorbent performance while avoiding misleading cross-metal generalizations. Importantly, the high removal efficiencies achieved—even in

the presence of competitive ions—underscore the applicability of these sustainable sorbents for complex water treatment scenarios.

The high adsorption capacity observed, especially for Cd and Fe ions, also reflects the competitive nature of multielement adsorption. However, the relatively high adsorption capacities observed for Cd(II) and total iron (Fe_{tot}) may be attributed not only to their higher initial concentrations in the multicomponent solution but also to their distinct physicochemical characteristics. Cd(II), with its small hydrated radius and divalent nature, demonstrates a strong affinity toward negatively charged adsorption sites. In the case of Fe_{tot}, present predominantly as Fe(III), the enhanced adsorption is likely due to the high binding affinity of trivalent iron ions to oxygen-containing functional groups such as hydroxyl and carboxyl moieties, particularly at moderately acidic to near-neutral pH values.

While some studies report reduced capacity under similar adsorption conditions [34], the biochars investigated here retained high removal efficiencies, highlighting their promise for real-world wastewater treatment. The presence of multiple metal ions in solution introduces competitive adsorption dynamics, where species with higher binding affinities or greater concentrations may dominate sorption sites. The observed selectivity patterns suggest a complex interplay between ion properties—such as charge density, ionic radius, and hydration energy—and the physicochemical characteristics of the biochar surface. Understanding these interactions is crucial for predicting sorbent behavior in real wastewater systems. This outcome is particularly notable given the use of low, environmentally relevant contaminant concentrations, which naturally limit Q_e values but offer a realistic assessment of practical sorbent performance. It should also be noted that the maximum monolayer adsorption capacity (Q_{max}) was not determined, as the study was based on adsorption data collected at a single equilibrium concentration for each metal ion. As a result, it is not possible to assess whether adsorption occurred near saturation or within the initial linear region of the isotherm. In cases with higher initial metal concentrations, the elevated Q_e values may reflect more extensive surface coverage rather than stronger sorbent–sorbate interactions.

5. Conclusions

This study provides a comparative analysis of biochars derived from AS, WS, PS, and RH, synthesized via slow pyrolysis at 793 K. The materials exhibited distinct physicochemical properties shaped by the composition and structure of the respective feedstocks. AS-BC, WS-BC, and PS-BC showed relatively high specific surface areas, with PS-BC reaching a maximum of 440 m^2/g. These values are attributed to the lignin-rich and mechanically dense nature of the nutshell precursors. Morphological observations revealed that AS-BC and PS-BC developed well-organized macroporous networks, whereas WS-BC displayed a more irregular structure with limited pore connectivity. RH-BC retained the characteristic framework of the original biomass and exhibited a predominantly mesoporous texture. Textural analysis confirmed that AS-BC, WS-BC, and PS-BC were predominantly microporous, with over 77% of their total pore volume in the micropore range—a key factor in their enhanced adsorption performance. In contrast, RH-BC demonstrated a type IV isotherm with an H3 hysteresis loop, indicative of mesoporosity arising from its silica-rich composition and broader pore size distribution.

The adsorption behavior of the biochars toward Cd(II), Mn(II), Co(II), Ni(II), Zn(II), Fe_{tot}, As_{tot}, and Cr_{tot} in multicomponent aqueous systems was strongly influenced by both the solution pH and the structural characteristics of the sorbents. Removal efficiencies ranged from 87.4% to 99.9%. Among the materials tested, WS-BC showed the highest affinity for Fe_{tot} and Cd(II), along with effective removal of Mn(II) and Co(II). PS-BC

also demonstrated strong adsorption potential across multiple metal ions, reflecting the influence of its high surface area and microporous architecture.

The study highlights the key influence of feedstock composition, particularly lignin content, structural rigidity, and mineral profile, on biochar porosity and adsorption efficiency. The results of this study align closely with the core principles of the circular economy by demonstrating the successful valorization of agricultural waste materials—traditionally underutilized residues—into functional sorbents for environmental remediation. The biochars produced not only offer a low-cost and renewable alternative to conventional adsorbents, but also hold potential for reuse or regeneration, contributing to resource efficiency and waste minimization. This closed-loop approach supports the development of sustainable water treatment strategies within the broader framework of circular economy thinking.

Author Contributions: All authors contributed equally to the conceptualization, methodology, validation, formal analysis, data visualization, and writing and editing of the original draft manuscript. All authors have read and agreed to the published version of the manuscript.

Funding: This work was supported financially by Project BG05M2OP001-1.002-0019: 'Clean Technologies for Sustainable Environment—Waters, Waste, Energy for a Circular Economy', funded by Operational Program 'Science and Education for Smart Growth', co-funded by the European Union through the European Structural and Investment Funds.

Informed Consent Statement: Not applicable.

Data Availability Statement: The supporting information and raw experimental data could be provided by the corresponding author upon request.

Conflicts of Interest: The authors declare no conflicts of interest.

References

1. IARC. *Agents Classified by the IARC Monographs*; IARC: Lyon, France, 2016; Volumes 1–116.
2. Tchounwou, P.B.; Yedjou, C.G.; Patlolla, A.K.; Sutton, D.J. Molecular, clinical and environmental toxicicology Volume 3: Environmental Toxicology. *Mol. Clin. Environ. Toxicol.* **2012**, *101*, 133–164.
3. Pan, J.; Plant, J.A.; Voulvoulis, N.; Oates, C.J.; Ihlenfeld, C. Cadmium levels in Europe: Implications for human health. *Environ. Geochem. Health* **2010**, *32*, 1–12. [CrossRef] [PubMed]
4. Godt, J.; Scheidig, F.; Grosse-Siestrup, C.; Esche, V.; Brandenburg, P.; Reich, A.; Groneberg, D.A. The toxicity of cadmium and resulting hazards for human health. *J. Occup. Med. Toxicol.* **2006**, *1*, 22. [CrossRef]
5. Faroon, O.; Annette, A.; Wright, S.; Tucker, P.; Jenkins, K. *Toxicological Profile for Cadmium*; Agency for Toxic Substances and Disease Registry: Atlanta, GA, USA, 2012.
6. McMillan, D.E. A brief history of the neurobehavioral toxicity of manganese: Some unanswered questions. *Neurotoxicology* **1999**, *20*, 499–507. [PubMed]
7. Seilkop, S.K.; Oller, A.R. Respiratory cancer risks associated with low-level nickel exposure: An integrated assessment based on animal, epidemiological, and mechanistic data. *Regul. Toxicol. Pharmacol.* **2003**, *37*, 173–190. [CrossRef]
8. Schaumlöffel, D. Nickel species: Analysis and toxic effects. *J. Trace Elem. Med. Biol.* **2012**, *26*, 1–6. [CrossRef]
9. Zamora-Ledezma, C.; Negrete-Bolagay, D.; Figueroa, F.; Zamora-Ledezma, E.; Ni, M.; Alexis, F.; Guerrero, V.H. Heavy metal water pollution: A fresh look about hazards, novel and conventional remediation methods. *Environ. Technol. Innov.* **2021**, *22*, 101504. [CrossRef]
10. Oladoye, P.O. Natural, low-cost adsorbents for toxic Pb(II) ion sequestration from (waste) water: A state-of-the-art review. *Chemosphere* **2022**, *287*, 132130. [CrossRef]
11. Kumkum, P.; Kumar, S. A Review on Biochar as an Adsorbent for Pb(II) Removal from Water. *Biomass* **2024**, *4*, 243–272. [CrossRef]
12. Macedo, J.C.A.; Shirinkar, M.; Landers, R.; Rosa, A.H. Exploring Biomass Waste-Derived Biochar as a Catalyst for Levulinic Acid Conversion to γ-Valerolactone: Insights into Synthesis, Characterization, and Catalytic Performance. *Biomass* **2025**, *5*, 29. [CrossRef]
13. Joseph, N.T.; Chinonye, O.E.; Philomena, I.K.; Christian, A.C.; Elijah, O.C. Isotherm and kinetic modeling of adsorption of dyestuffs onto kola nut (*Cola acuminata*) shell activated carbon. *J. Chem. Technol. Metall.* **2016**, *51*, 188–201.

14. Tariq, W.; Arslan, C.; Tayyab, N.; Rashid, H.; Nasir, A. *Application of Agro-Based Adsorbent for Removal of Heavy Metals*, 1st ed.; Elsevier Ltd.: Amsterdam, The Netherlands, 2022.
15. Kali, A.; Amar, A.; Loulidi, I.; Jabri, M.; Hadey, C.; Lgaz, H.; Alrashdi, A.A.; Boukhlifi, F. Characterization and adsorption capacity of four low-cost adsorbents based on coconut, almond, walnut, and peanut shells for copper removal. *Biomass Convers. Biorefinery* **2022**, *14*, 3655–3666. [CrossRef]
16. *ISO 9277:2010*; Determination of the Specific Surface Area of Solids by Gas Adsorption-BET Method. ISO: Geneva, Switzerland, 2010.
17. Vlaev, L. *Adsorption and Catalysis*; Baltika-2002: Burgas, Bulgaria, 2014.
18. Stoeckli, F.; López-Ramón, M.; Hugi-Cleary, D.; Guillot, A. Micropore sizes in activated carbons determined from the Dubinin–Radushkevich equation. *Carbon* **2001**, *39*, 1115–1116. [CrossRef]
19. *BDS, EN ISO 17294-2: 2016*; Water Quality—Application of Inductively Coupled Plasma Mass Spectrometry (ICP-MS)—Part 2: Determination of Selected Elements Including Uranium Isotopes. ISO: Geneva, Switzerland, 2016.
20. Gonsalvesh, L.; Marinov, S.P.; Gryglewicz, G.; Carleer, R.; Yperman, J. Preparation, characterization and application of polystyrene based activated carbons for Ni(II) removal from aqueous solution. *Fuel Process. Technol.* **2016**, *149*, 75–85. [CrossRef]
21. Zeng, F.; Li, Z.; Li, X.; Wang, J.; Kong, Z.; Sun, Y.; Liu, Z.; Feng, H. Almond-derived origami-like hierarchically porous and N/O co-functionalized carbon sheet for high-performance supercapacitor. *Appl. Surf. Sci.* **2019**, *467–468*, 229–235. [CrossRef]
22. Liu, S.T.; Chen, X.G.; Zhang, A.B.; Yan, K.K.; Ye, Y. Electromagnetic Performance of Rice Husk Ash. *BioResources* **2014**, *9*, 2328–2340. [CrossRef]
23. Bhavani, P.; Kumar, D.P.; Hussain, M.; Aminabhavi, T.M.; Park, Y.K. Eco-friendly rice husk derived biochar as a highly efficient noble Metal-Free cocatalyst for high production of H2 using solar light irradiation. *Chem. Eng. J.* **2022**, *434*, 134743. [CrossRef]
24. Genieva, S.; Gonsalvesh, L.; Georgieva, V.; Tavlieva, M.; Vlaev, L. Kinetic analysis and pyrolysis mechanism of raw and impregnated almond shells. *Thermochim. Acta* **2021**, *698*, 178877. [CrossRef]
25. Ye, Y.; Liang, L.; Zhang, X.; Sun, J. Simple carbonaceous-material-loaded mesoporous SiO_2 composite catalyst for epoxide-CO_2 cycloaddition reaction. *J. Colloid Interface Sci.* **2022**, *610*, 818–829. [CrossRef]
26. Xiao, R.; Yang, W. Influence of temperature on organic structure of biomass pyrolysis products. *Renew. Energy* **2013**, *50*, 136–141. [CrossRef]
27. Adamczyk, A. Effects of applying different type SiO_2 precursors on the structure of selected zirconia-silica gels. *J. Mol. Struct.* **2022**, *1264*, 133143. [CrossRef]
28. Heakal, F.E.-T.; Abd-Ellatif, W.R.; Tantawy, N.S.; Taha, A.A. Impact of pH and temperature on the electrochemical and semiconducting properties of zinc in alkaline buffer media. *RSC Adv.* **2018**, *8*, 3816–3827. [CrossRef] [PubMed]
29. Duranoglu, D.; Beker, U. Cr(VI) Adsorption Onto Biomass Waste Material-Derived Activated Carbon. In *Desalination Updates*; IntechOpen: London, UK, 2015.
30. Niazi, N.K.; Bibi, I.; Shahid, M.; Ok, Y.S.; Shaheen, S.M.; Rinklebe, J.; Wang, H.; Murtaza, B.; Islam, E.; Nawaz, M.F.; et al. Arsenic removal by Japanese oak wood biochar in aqueous solutions and well water: Investigating arsenic fate using integrated spectroscopic and microscopic techniques. *Sci. Total Environ.* **2018**, *621*, 1642–1651. [CrossRef]
31. Lima, I.M.; Boateng, A.A.; Klasson, K.T. Physicochemical and adsorptive properties of fast-pyrolysis bio-chars and their steam activated counterparts. *J. Chem. Technol. Biotechnol.* **2010**, *85*, 1515–1521. [CrossRef]
32. Singh, E.; Kumar, A.; Mishra, R.; You, S.; Singh, L.; Kumar, S.; Kumar, R. Pyrolysis of waste biomass and plastics for production of biochar and its use for removal of heavy metals from aqueous solution. *Bioresour. Technol.* **2021**, *320*, 124278. [CrossRef]
33. Chen, W.H.; Hoang, A.T.; Nižetić, S.; Pandey, A.; Cheng, C.K.; Luque, R.; Ong, H.C.; Thomas, S.; Nguyen, X.P. Biomass-derived biochar: From production to application in removing heavy metal-contaminated water. *Process Saf. Environ. Prot.* **2022**, *160*, 704–733. [CrossRef]
34. Neris, J.B.; Luzardo, F.H.M.; da Silva, E.G.P.; Velasco, F.G. Evaluation of adsorption processes of metal ions in multi-element aqueous systems by lignocellulosic adsorbents applying different isotherms: A critical review. *Chem. Eng. J.* **2019**, *357*, 404–420. [CrossRef]

Disclaimer/Publisher's Note: The statements, opinions and data contained in all publications are solely those of the individual author(s) and contributor(s) and not of MDPI and/or the editor(s). MDPI and/or the editor(s) disclaim responsibility for any injury to people or property resulting from any ideas, methods, instructions or products referred to in the content.